Original article
DOI: https://doi.org/10.18721/JPM.15406

THE STRUCTURE OF A 3D FLOW WITH LOCAL TURBULENCE IN THE BRANCHING JUNCTURE OF A CIRCULAR-SECTION CHANNEL

Ya. A. Gataulin[1]✉, *E. M. Smirnov*[1], *V. M. Molochnikov*[2,3], *A. N. Mikheev*[3]

[1] Peter the Great St. Petersburg Polytechnic University, St. Petersburg, Russia;

[2] Kazan National Research Technical University named after A. N. Tupolev – KAI, Kazan, Russia;

[3] FRC "Kazan Scientific Center of RAS", Kazan, Russia

✉ yakov_gataulin@mail.ru

Abstract. The paper presents the results of a computational and experimental studies of a flow with local turbulence in the branching juncture of a channel with a round cross-section for the inlet Reynolds number Re = 1475 and for equal flow rates in two branches. The numerical solution of the problem has been obtained by the LES technique using the Germano − Lilli dynamic model for estimating the subgrid viscosity. The experiment used the SIV method. The calculated and experimental data in agreement showed that a jet-flow zone and a recirculation one were distinguished in the flow, directly in the branching juncture both in the forward and in the side channels. Turbulent stresses were significant in magnitude only in the channel section about four gauges long. Downstream, the flow in both channels was relaminarized.

Keywords: blood flow branching, local turbulence, large eddy simulation, SIV measurements

Funding: The reported study was funded by Russian Science Foundation (Grant No. 20-65-47018).

Citation: Gataulin Ya. A., Smirnov E. M., Molochnikov V. M., Mikheev A. N., The structure of a 3D flow with local turbulence in the branching juncture of a circular-section channel, St. Petersburg State Polytechnical University Journal. Physics and Mathematics. 15 (4) (2022) 81–94. DOI: https://doi.org/10.18721/JPM.15406

Научная статья
УДК 532.542.4
DOI: https://doi.org/10.18721/JPM.15406

СТРУКТУРА ТРЕХМЕРНОГО ТЕЧЕНИЯ С ЛОКАЛЬНОЙ ТУРБУЛЕНТНОСТЬЮ В ОБЛАСТИ РАЗВЕТВЛЕНИЯ КАНАЛА КРУГЛОГО СЕЧЕНИЯ

Я. А. Гатаулин[1]✉, *Е. М. Смирнов*[1], *В. М. Молочников*[2],*З*, *А. Н. Михеев*[3]

[1] Санкт-Петербургский политехнический университет Петра Великого, Санкт-Петербург, Россия;

[2] Казанский национальный исследовательский технический университет имени А. Н. Туполева – КАИ, г. Казань, Россия;

[3] Федеральный исследовательский центр «Казанский научный центр Российской академии наук», г. Казань, Россия

✉ yakov_gataulin@mail.ru

Аннотация. Статья представляет результаты расчетно-экспериментального исследования течения с локальной турбулентностью в области разветвления канала круглого сечения, при входном числе Рейнольдса Re = 1475 и равном распределении расхода по двум ветвям. Численное решение задачи получено методом моделирования крупных вихрей (LES) по динамической модели Джермано − Лилли для оценки подсеточной вязкости. Эксперимент выполнен с использованием метода SIV. Находящиеся в согласии расчетные и опытные данные показывают, что непосредственно в области разветвления, как в прямом, так и в боковом каналах, в потоке выделяются зона струйного течения и рециркуляционная зона. Турбулентные напряжения значительны по величине лишь на участке длиной около четырех калибров. Вниз по потоку течение в обоих каналах реламинаризируется.

Ключевые слова: разветвление кровотока, локальная турбулентность, метод моделирования крупных вихрей, SIV-измерения

Финансирование: Работа выполнена при финансовой поддержке Российского научного фонда (РНФ), грант № 20-65-47018.

Для цитирования: Гатаулин Я. А., Смирнов Е. М., Молочников В. М., Михеев А. Н. Структура трехмерного течения с локальной турбулентностью в области разветвления канала круглого сечения // Научно-технические ведомости СПбГПУ. Физико-математические науки. 2022. Т. 15. № 4. С. 81–94. DOI: https://doi.org/10.18721/JPM.15406

Introduction

Branched pipeline networks are widely used to transport liquids and gases in engineering practice, for example, in internal combustion engines, compressors, hydraulic turbines, etc. Due to the typical sizes of these devices and their operational modes with high Reynolds numbers, the flow throughout the pipeline network bears a pronounced turbulent character.

The situation is somewhat different for hemodynamics of the human cardiovascular system. Blood flow in most of the main vessels (arteries) is characterized by moderate Reynolds numbers (about 10^3). For this reason, there are multiple aspects to the problem of turbulent structures evolving in the vascular bed, accompanied by sharp changes in the flow channel of the vessel or the direction of blood flow, including branching cases.

Natural bifurcations (branching) of the arteries are typical sites with increased risk for occurrence and development of atherosclerosis, one of the most common diseases that can lead to ischemic stroke, long-term disability or even death. All of this attracts attention towards detailed study of three-dimensional dynamics of blood flow in branched arteries [1–3]. A region with branching is sometimes artificially constructed in the vascular bed during surgeries to implant a shunt/prosthesis restoring blood flow through an artery that is locally blocked by the developing abnormalities. Neointimal hyperplasia, i.e., excessive proliferation of inner layers of vascular tissue (intima) in the suture site leading to prosthesis occlusion, may develop over time in end-to-side anastomoses (connection between the prosthesis and the vessel).

Low wall shear stress (WSS) is generally believed to be the main cause behind the production of atherosclerotic plaques and neointimal thickening. This is corroborated by numerous studies. Aside from the magnitude of the WSS, the dynamics of this parameter also considerably affect the proliferation of the inner wall layer in the affected vessel: high time-averaged spatial WSS gradients (WSSG) correlate with accelerated plaque formation and intimal thickening [4–6].

Abnormally high or low values of skin friction in the vascular junction with branching are due to complex 3D dynamics of the flow. Local turbulence of the flow around the vascular branching can affect such important parameters as the position and size of the recirculation region, the intensity of the fluctuations in the blood flow parameters, including WSS. This, in turn, affects the biochemical processes in endothelial cells and can lead to intense intimal proliferation and consequent occlusion of the prosthesis.

Extensive, primarily numerical, studies have focused on the vortical structure of the flow and its transition to turbulence (or emergence of regions with local turbulence) in models of stenotic blood vessels [7–15]. In contrast, only scarce systematic analysis is available for local turbulence in branching junctions of channels, as well as for the evolution of 3D flow in these regions at Reynolds numbers of the order of 10^3.

A notable recent paper [16] reports on numerical simulation of fully developed turbulent flow (for Reynolds numbers of the order of 10^6) and head losses in the region where the main pipe with a round cross section bifurcates into a leg with a slightly smaller diameter.

The computations and experiments carried out in our study were aimed at describing the dynamics of separation flow and turbulent blood flow evolving in end-to-side vascular anastomoses.

In addition to experimental study, we performed numerical simulation of largely steady flow in a branched channel, with the Reynolds number Re = 1475 close to the maximum (according to statistical data) for blood flow in the human femoral artery over the cardiac cycle.

Experimental

The schematic of the experimental setup is shown in Fig. 1. The flow in the test section of the setup is generated by the pressure head from the pressure vessel *1* mounted on a rigid frame. Liquid in this vessel (constant pressure head) is maintained at a constant level by means of decanter *2* and pump *9*, which pumps liquid from storage tank *7* into the pressure vessel. The liquid from the pressure tank enters test section *10* through dispenser *3* with a set of nozzles with different cross-sectional areas. The required flow rate of the working fluid is set by switching to a specific group of nozzles. The test section is a channel with a branching. The flow rates of the liquid flowing through the main section and the branch are regulated by throttle valves *13* installed in drain pipes *12*. The corresponding flow rates are controlled by directly measuring the weight of the liquid flowing over the required period of time through the drain pipes to the measuring tanks installed on strain gauge balance *14*.

The setup allows for experiments with both steady and pulsatile flow. Flow rate fluctuations are generated in the test section of the setup through reciprocating motion of piston *4*, triggered by disk-shaped cam *5*, which is rotated by electric motor *6* with a frequency converter.

The setup is equipped with a system for measuring instantaneous two-dimensional vector fields of the flow velocity (Smoke Image Velocimetry (SIV)) [17]. Polyamide particles 5 μm in diameter are used as tracers. A higher concentration of tracers, compared with the digital method for tracer visualization of flows (Particle Image Velocimetry (PIV)), aimed at increasing spatial resolution and reducing measurement noise.

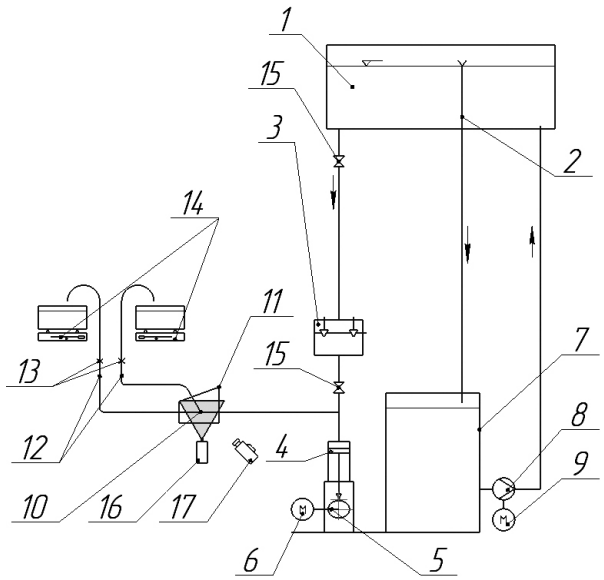

Fig. 1. Schematic of experimental setup for studying the fluid flow in a channel with a side branch: pressure vessel *1*; decanter system *2*; dispenser *3*; piston *4*; cam *5*; electric motor *6* with frequency converter; storage tank *7*; pump *8*; electric drive *9*; test section *10*; box *11*; drain pipes *12*; throttle valves *13*; measuring tanks *14* with strain gauge scales; shutoff valves *15*; laser *16*; high-speed camera *17*

The test section of the setup is a smooth pipe with a branch installed at an angle of 60° (Fig. 2). The inner diameter of the main pipe and the branch made of transparent polycarbonate is $D = 17$ mm. An aqueous solution of glycerin with a mass fraction of 56.3% is used as a working fluid. The test section was placed in glycerin-filled box *11*, shaped as a rectangular parallelepiped, to reduce the measurement error due to the difference in the refractive coefficients of the working fluid and air.

PIV visualization of the flow was carried out in the symmetry plane of the test section using an Evercam 2000-4M high-speed camera with a light sheet generated by an SSP-ST-532-NB-5-5-LED-VAC CW laser (wavelength of 532 nm (bright green)). A traverse system was used to position the camera and the laser across the test section.

The temperature of the working fluid in the experiments was varied by no more than 0.5 °C, and it was controlled with a TPTU-1-1-100-142/0...100-0.25 certified thermal sensor. The fluid viscosity in the experimental conditions was $\nu = 7.85 \cdot 10^{-6}$ m^2/s, and it was controlled before each series of experiments by direct measurements via a capillary viscometer (viscometer for transparent liquids) with a margin of error of 0.35%.

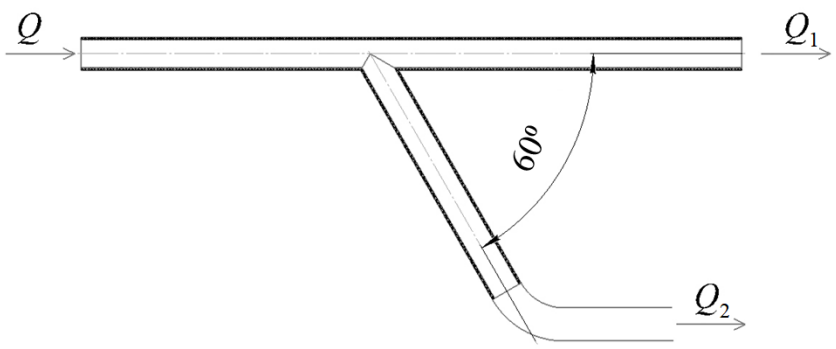

Fig. 2. Schematic test section of experimental setup (see *10* in Fig. 1): Q, Q_1, Q_2 are the flow rates through the main channel and the branch

The experiments were carried out assuming a largely steady flow of the working fluid at the Reynolds number Re = 1475, computed from the average inlet velocity U_b and diameter D. The ratio of flow rates through the main channel and the branch was $Q_1/Q = Q_2/Q = 0.5$.

Aspects of numerical simulation

The geometry of the computational domain (Fig. 3) in the numerical simulation fully corresponded to the test section of the experimental setup. Fig. 3 shows the two coordinate systems introduced. The origin of the Cartesian system x, y, z for the main channel is located in the symmetry plane, on the wall with the adjacent side channel, at a distance equal to one diameter D of the channel (one gauge) from the branching junction (the vertex of an obtuse angle); the x axis is directed along the flow. The origin of the Cartesian coordinate system $\hat{x}$, $\hat{z}$, $\hat{z}$, introduced for the side channel, is located at the vertex of the obtuse angle (at the beginning of the branching); the axis $\hat{y}$ is directed along the outer wall of the side channel, and the axis $\hat{y}$ is directed towards the inner wall (forming an acute angle with the inner wall of the main channel). The computational domain included an inlet section with the length L_1 equal to $10D$, a section of the main (straight) channel after branching with the length $L_2 = 10D$ and a side channel with the outer wall length L_3 also equal to $10D$. The chosen lengths L_2 and L_3 are sufficient provided there is no effect from artificial boundary conditions imposed at the outlets from the computational domain.

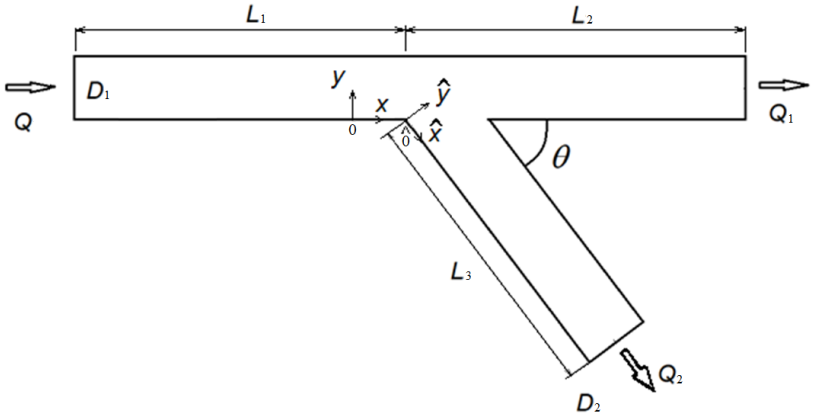

Fig. 3. Schematic of computational domain adopted for numerical simulation; the geometry of the domain and the two coordinate systems introduced are shown
D_i are the channel diameters, $L_1 = L_2 = L_3 = 10D$

Numerical simulation for the given flow of incompressible viscous fluid with a constant viscosity was performed by Large Eddy Simulation (LES) using the dynamic Germano–Lilly model [18, 19]. The computations were carried out using the general-purpose finite-volume ANSYS CFX 18.2 code; the hydrodynamic equations are solved in terms of dimensional quantities.

A velocity distribution corresponding to the Poiseuille profile for well-developed laminar flow in a round pipe was set at the inlet to the computational domain. The mean inlet velocity U_b was selected to satisfy the condition imposed for the experiment that the Reynolds number Re = 1475. Constant pressure and 'soft' boundary conditions for the velocity were imposed at the outlet Q_1 (see Fig. 3), the condition for a given flow rate (50% of the inlet) was imposed at the outlet Q_2. The no-slip condition was imposed on the walls.

An O-grid-type computational mesh consisting of hexahedral blocks was constructed in ICEM CFD software (fragments of the mesh are shown in Fig. 4). The longitudinal mesh spacing was $0.03D$ in the branching junction, while the maximum transverse spacing was $0.01D$. The total number of elements in the mesh was about 6.5 million. A central scheme with second-order accuracy was used in the computations to approximate the convective terms of the equations of motion, and a three-layer Euler scheme was used for time derivatives. The time step was $0.0053t_s$ (t_s is the time scale of the problem, $t_s = D/U_b$); this step was selected to provide the local values of the Courant number less than unity over the entire computational domain.

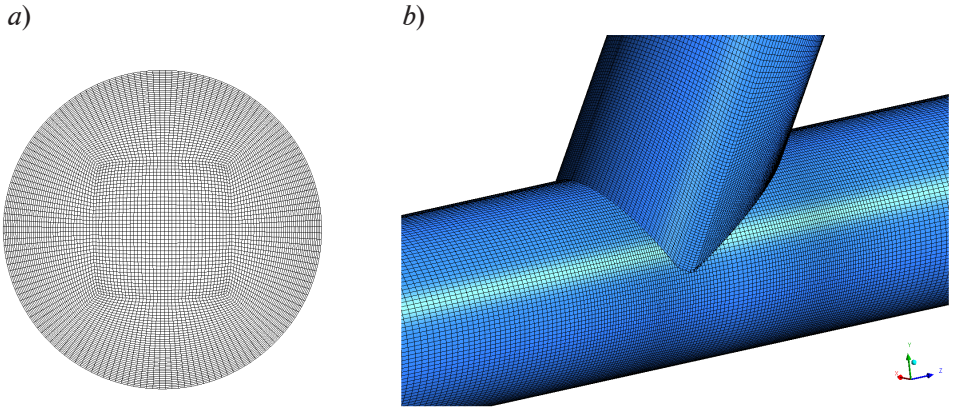

Fig. 4. Computational mesh in cross section (*a*) and in the branching junction (*b*)

The sample used to obtain the averaged flow characteristics was accumulated over a time period equal to $1050t_s$; the previous time interval, covering about $600t_s$, was sufficient to generate statistically steady flow, starting from a zero velocity field.

The simulations were run on the Polytechnic RSC Tornado cluster of the Polytechnic Supercomputer Center (http://www.scc.spbstu.ru). The problem was run on 18 dual-core nodes (Intel (R) Xeon (R) E5 2697v3) and parallelized to 450 cores; the full simulation took about a week of real time (76,000 core hours).

Analysis and discussion of the data obtained

Flow patterns obtained by visualization of experimental and computational data are shown in Fig. 5. Computations and experiments yield a similar structure of the flow. The flow is lamina before the branching, with shear layers losing stability further downstream and the flow subsequently becoming turbulent. Very strong jets propagate along the inner walls of the branching junction (forming an acute angle), the zones with turbulent flow are adjacent to the opposite (outer) walls.

The time-averaged longitudinal (axial) velocity component and its RMS fluctuation in the main channel are denoted as U and u_{rms}, and similar quantities in the side channel are denoted by the same symbols with a cap, i.e., $\hat{U}, \hat{u}_{rms}$.

Fig. 6 shows the isosurface of the Q-criterion [20]; the colors correspond to the local values of the RMS fluctuations of longitudinal velocity, visualizing the localized regions with turbulent flow filled with multi-scale vortical structures observed in the branching junction.

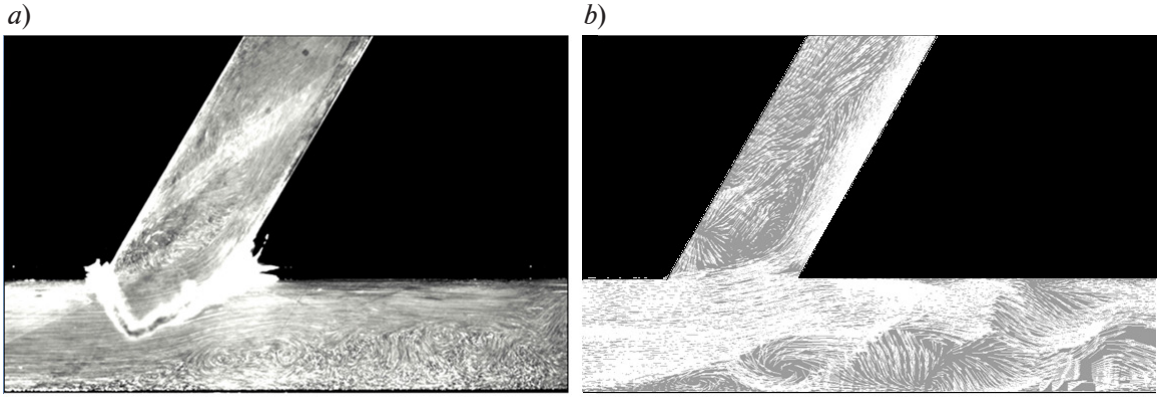

Fig. 5. Visualization of the flow in the symmetry plane of the channel:
SIV measurement results (*a*), computed field of the velocity vector (*b*)

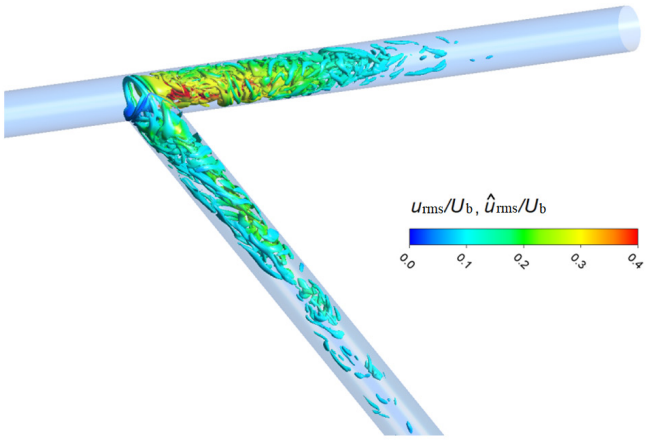

Fig. 6. Isosurface of the Q-criterion; the colors correspond to the root-mean-square fluctuations of longitudinal velocity in the two branches of the channel

Measurements of the time-averaged longitudinal velocity and its fluctuations were performed in the central plane (symmetry plane) in the cross sections of the flow channel with the following normalized coordinates:

for a straight channel,

$$x/D = 0.00;\ 1.00;\ 1.58;\ 1.77;\ 2.17;\ 2.56;\ 3.15;\ 3.55;\ 4.34;\ 4.93;$$

for the side channel,

$$\hat{x}/D = 0.00;\ 0.20;\ 0.39;\ 0.59;\ 0.79;\ 1.38;\ 2.17;\ 2.76;\ 3.35.$$

The measured profiles of longitudinal velocity and its fluctuations were used to construct two-dimensional fields of these quantities (Fig. 7) by the interpolation procedure in the Tecplot360 program against the computational data.

Comparing the computational and experimental fields of the longitudinal velocity component (Fig. 7), we find that the data are in good qualitative agreement. Two main regions were detected in the flow behind the branching junction: high-speed jets near the inner walls and recirculation zones near the outer walls of the branching junction. However, computations indicate that reverse flow is more intense in the recirculation zones in the straight and side channels; consequently, the computed recirculation zone in the side channel is noticeably larger than the experimental one.

A high-speed jet appears after the junction near the inner wall of the main channel. The maximum velocity in the jet is almost 1.5 times higher than the mean flow velocity U_b in the channel before the junction and, accordingly, almost 3 times higher than the local mean flow velocity equal to 0.5 U_b accounting for the fact that half the flow is directed into the side channel. The jet quickly loses its intensity downstream. According to computations and measurements, the longitudinal size of the recirculation zone in the straight channel is approximately 3.2 and 4.0 channel gauges, respectively.

Significant transverse gradients of the flow velocity are observed in the shear layers evolving at the boundary between the jet and the low-velocity region. The shear layers lose their stability in these conditions. As nonlinear hydrodynamic processes develop, the maximum in the fluctuations of the longitudinal velocity component increases, reaching $u_{rms}/U_b \approx 0.45$ for the straight channel and $\hat{u}_{rms}/U_b \approx 0.20$ for the side channel in the computations (Fig. 7, *c, d*). The distribution of fluctuation intensity becomes close to uniform in the main channel at $x/D > 5$, while the field of $\hat{u}_{rms}$ remains divided into two layers with different levels of fluctuation intensity for a relatively long time in the side channel. Experimental data point to the same trends, but the maximum level of longitudinal velocity fluctuations in the straight channel is about 30% lower.

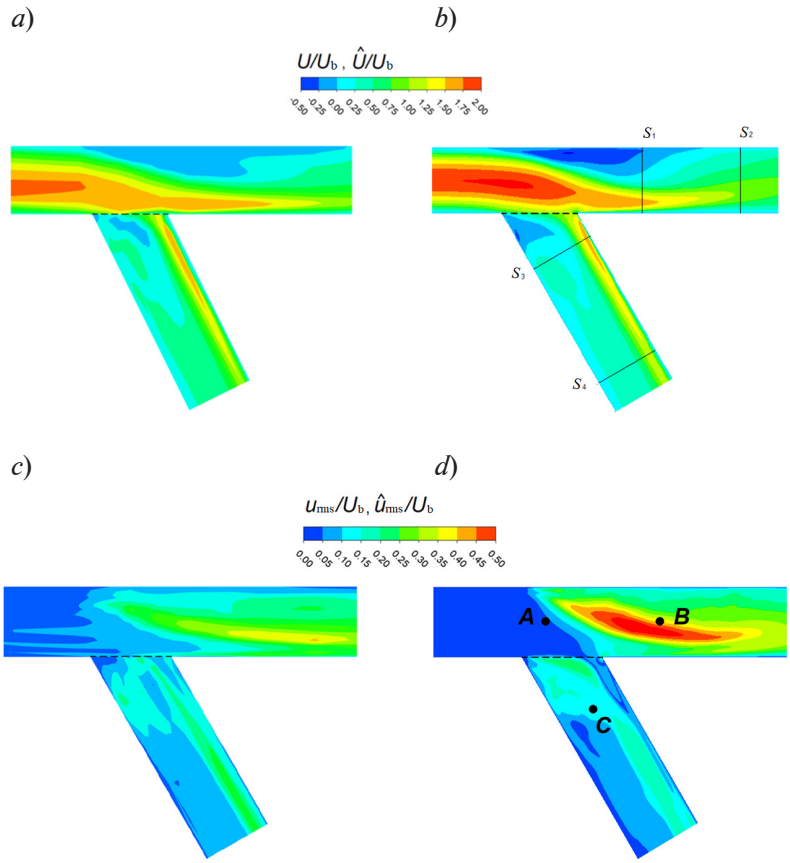

Fig. 7. Fields of time-averaged longitudinal velocity component (*a*, *b*) and RMS fluctuations of this component (*c*, *d*): *a*, *c* correspond to the experiment; *b*, *d* to the computations

Fig. 8 compares the experimental profiles of averaged longitudinal velocity with the results of numerical simulation at $x/D = 0.00$, 1.58 and 3.15 for the straight channel and $\hat{x}/D = 2.76$ for the side channel. Measurements of the longitudinal flow velocity at a distance of one gauge to the branching junction (Fig. 8, *a*) produced a significant difference from the profile for developed laminar flow in a round pipe (Poiseuille profile). Conversely, the computations indicate that the velocity distribution in this cross section has little difference from the Poiseuille profile set as a boundary condition at the inlet to the computational domain. A possible reason for the experimentally observed difference between the velocity profile at the inlet and the Poiseuille profile is the presence of residual secondary (transverse) flow initially evolving at the start of the primary straight channel when the flow passed through the t-junction (a honeycomb straightener was not installed at the inlet to this straight channel).

Analyzing the data in Fig. 8, we can conclude that satisfactory agreement between the computational and experimental results is reached downstream for the inlet velocity profile even despite this difference (see Fig. 8, *b*–*d*).

Because experimental data are scarce, only the results of numerical simulation are presented and discussed below to provide further insights into the three-dimensional structure of the given flow.

Fig. 9 shows the fields of averaged longitudinal velocity with superimposed fields of transverse velocity for four cross sections (S_1–S_4) of the model (marked by a solid line in Fig. 7,*b*). Furthermore, the jets that formed in the main and side channels are apparently characterized by relatively high local velocities (1.5 times higher than the large-scale velocity U_b). The flow after the junction is characterized by the presence of a significant transverse (secondary) flow that is a vortex pair in both branches (see Fig. 9, *a, c*). Secondary flow in the main channel weakens after two gauges, with the central pair of vortices replaced by a pair of vortices forming near the side

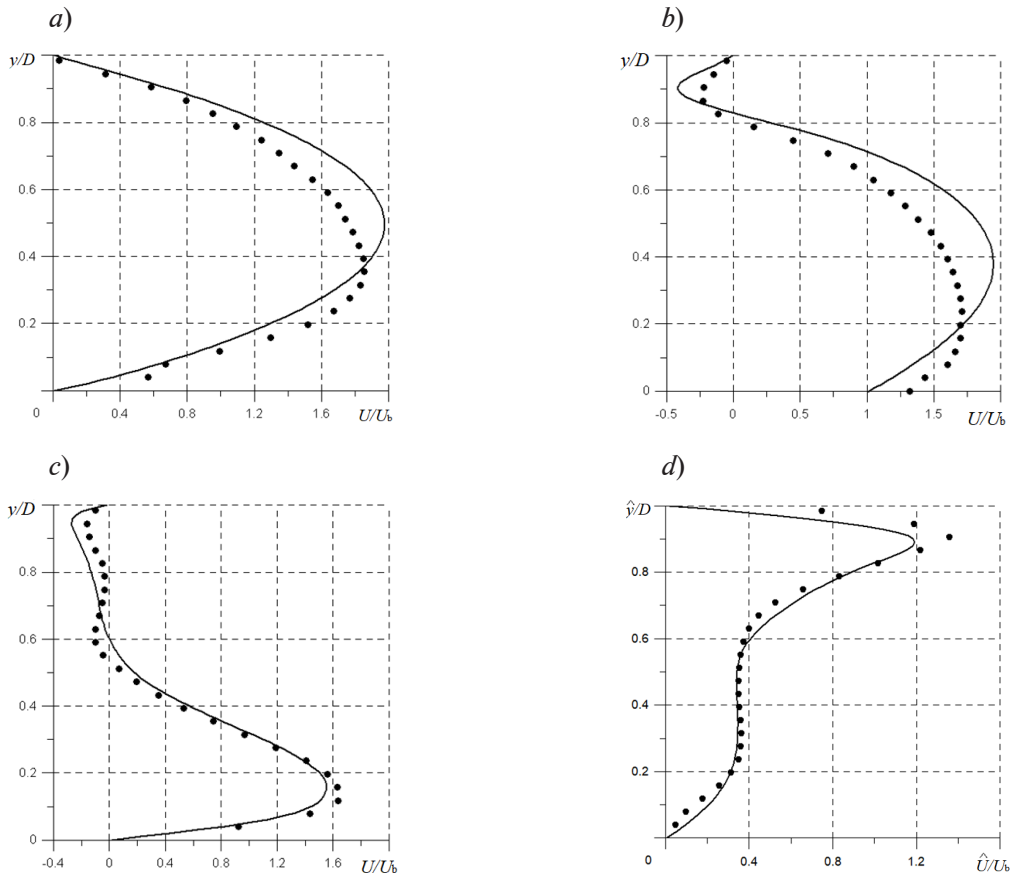

Fig. 8. Comparison of computational (lines) and experimental (points) profiles of time-averaged longitudinal flow velocity in the straight channel at different normalized coordinates of the cross sections x/D (*a*–*c*), and in the side channel at $\hat{x}/D = 2.76$ (*d*); $x/D = 0.00$ (*a*), 1.58 (*b*), 3.15 (*c*)

walls with reverse circulation (see Fig. 9,*b*).Secondary vortices gradually decay along the length of the side channel but preserve the direction of circulation in them. We should also note that transverse flow almost completely degenerates at a distance less than $10D$ after the junction, and the distribution of the averaged longitudinal velocity again acquires an axisymmetric 'pipe-like' appearance, with the maximum velocity in the center of the channel (the corresponding illustrations are not presented in Fig. 9).

Fig. 10 shows the time evolution of instantaneous longitudinal velocity at four points: two on the axes of the main and side channels (three of them are shown in Fig. 7,*d*). Interestingly, the flow at the very beginning of the branching junction, in particular near the intersection between the axes of the main and side channels, is quasi-periodic in nature (see Fig. 10,*a*) with the predominant dimensionless frequency $\mathrm{Sh} = fD/U_b \approx 0.51$. However, the flow shortly after the junction (Fig. 10, *b, d*) is characterized by irregular velocity fluctuations occurring as the flow moves past multi-scale vortical structures; the latter evolved as a result of local turbulence of the flow. The fluctuation amplitude decreases markedly further downstream (see Fig. 10,*c*).

Fig. 11 shows the longitudinal distributions of the time-averaged skin friction coefficient on the outer and inner walls of the channels (in the plane of symmetry). The skin friction coefficient was calculated by the formula

$$C_f = \tau_w \Big/ \left(\rho U_b^2 / 2\right),$$

where τ_w is magnitude of the skin shear stress on the wall.

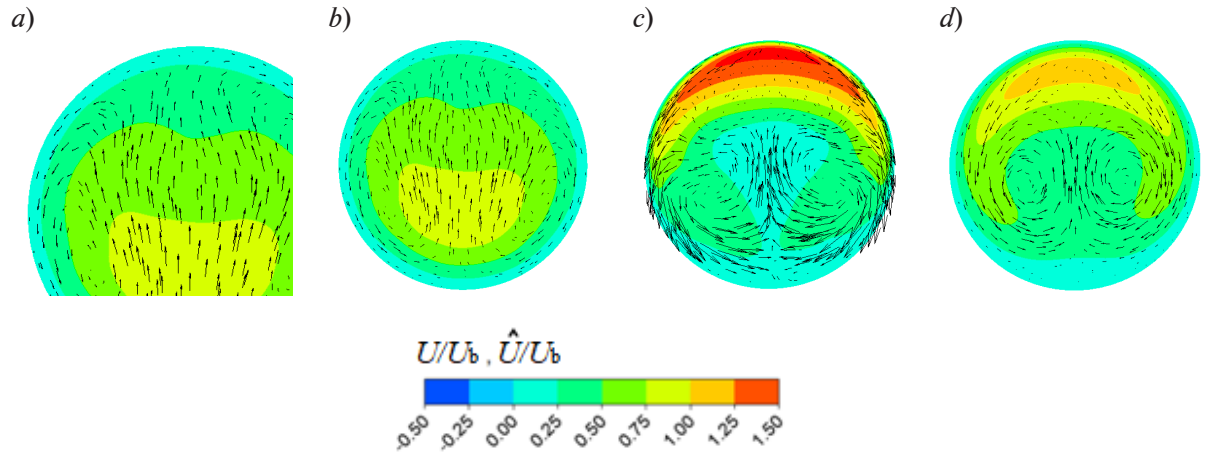

Fig. 9. Time-averaged longitudinal velocity fields with transverse velocity vector fields superimposed on them in four cross sections of the vessel model: $x/D = 3.15$ (*a*), 4.65 (*b*), $\hat{x}/D = 1$ (*c*) and 3 (*d*)

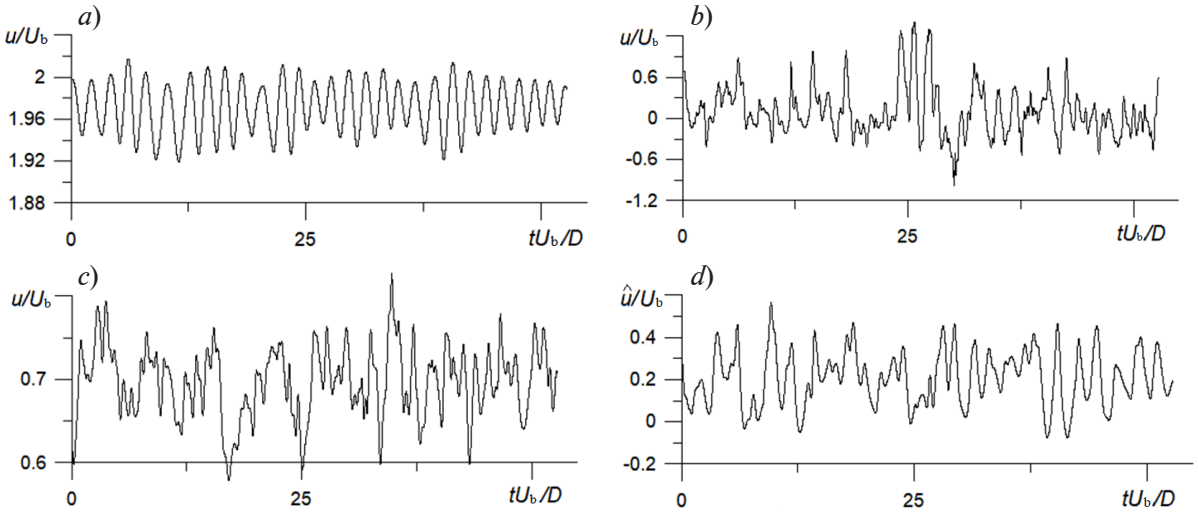

Fig. 10. Time evolution of instantaneous longitudinal flow velocity in the branching channel, computed for different points (see Fig. 7,*d*): *a*, in the center of the branching junction (point ***A***); *b*, *c*, at distances of $1.6D$ (point ***B***) and $10D$ (this point is not marked) from the branching center along the axis of the main channel; *d*, at a distance $1.4D$ from the center of the branching junction along the axis of the side channel (point ***C***)

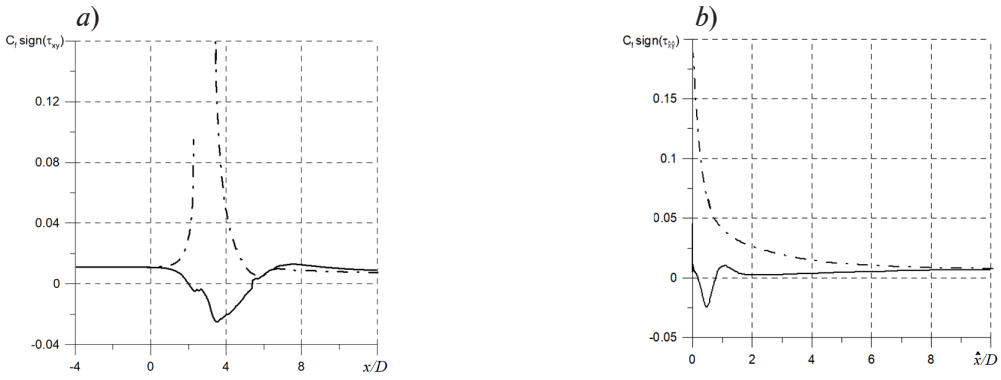

Fig. 11 Longitudinal variation of time-averaged skin friction coefficient in the main (*a*) and side (*b*) channels; data are given for external (solid line) and internal (dash-dotted line) branching walls

Regions with reverse flow were detected by computing the skin friction coefficients shown in the figures accounting for the sign of the longitudinal components τ_{xy} and $\tau_{\hat{x}\hat{y}}$ of the skin shear stress in the main and side channels.

The skin friction coefficient is relatively high on the inner channel walls around the branching, locally exceeding the value of 0.011 (by about 20 times) computed for a given Reynolds number for inlet laminar flow with a Poiseuille velocity profile.

The skin friction coefficient on the outer wall of the straight channel is comparable to the given value, and mostly lower by several times on the outer wall of the side channel.

The highest absolute values of the skin friction coefficient C_f in the regions with reverse flow are approximately two times higher than those in the inlet section.

Conclusion

We carried out physical experiments (by SIV measurements) and numerical simulation (LES method) to analyze largely steady flow in a circular channel with branching, with the Reynolds number Re = 1475 and a uniform distribution of the flow between two branches. The measurements and the computations yield results that are in good agreement, pointing to the following characteristics of the flow considered.

The laminar flow entering the branching region loses stability, consequently generating turbulence in this region, shedding multiscale vortices that completely fill the cross sections of both the main and the side channel. Rapid turbulence generation is caused by the emerging recirculation zones with separation flow and high-gradient mixing layers at their boundaries. Turbulent stresses are high in the zone about 4 gauges long, i.e., equal to the channel diameter. The flow in both channels is relaminarized downstream.

The time-averaged flow in each of the branches is characterized by a highly nonuniform longitudinal velocity field, with transverse motion represented by a pair of vortices that are rather intense in the first few gauges. The skin friction coefficient on the wall in the branching junction is also highly nonuniform; the values of this coefficient in some sites are either an order of magnitude higher than the value computed for the inlet flow, or vice versa, several times lower.

Combining the LES and SIV methods should undoubtedly improve the prediction quality for the characteristics of locally turbulent blood flow developing in end-to-side vascular anastomoses therefore yielding more reliable results for biomedical applications.

REFERENCES

1. **Schirmer C. M., Malek A. M.,** Computational fluid dynamic characterization of carotid bifurcation stenosis in patient-based geometries, Brain Behav. 2 (1) (2012) 42–52.

2. **Filardi V.,** Carotid artery stenosis near a bifurcation investigated by fluid dynamic analyses, Neuroradiol. J. 26 (4) (2013) 439–453.

3. **Li C-H., Gao B-L., Wang Ji-W., et al.,** Hemodynamic factors affecting carotid sinus atherosclerotic stenosis, World Neurosurg. 121 (2019) 262–276.

4. **Haruguchi H., Teraoka S. J.,** Intimal hyperplasia and hemodynamic factors in arterial bypass and arteriovenous grafts: a review, Artif. Organs. 6 (4) (2003) 227–235.

5. **McGah P. M., Leotta D. F., Beach K. W., et al.,** A longitudinal study of remodeling in a revised peripheral artery bypass graft using 3D ultrasound imaging and computational hemodynamics, J. Biomech. Eng. 133 (4) (2011) 1–10.

6. **Donadoni F., Pichardo-Almarza C., Bartlett M., et al.,** Patient-specific, multi-scale modeling of neointimal hyperplasia in vein grafts, Front. Physiol. 8 (2017) 1–10.

7. **Mittal R., Simmons S. P., Udaykumar H. S.,** Application of large-eddy simulation to the study of pulsatile flow in a modelled arteria stenosis, J. Biomech. Eng. 123 (4) (2001) 325–332.

8. **Mittal R., Simmons S. P., Najjar F.,** Numerical study of pulsatile flow in a constricted channel, J. Fluid Mech. 485 (2003) 337–378.

9. **Sherwin S. J., Blackburn H. M.,** Three-dimensional instabilities and transition of steady and pulsatile flows in an axisymmetric stenotic flows, J. Fluid Mech. 533 (2005) 297–327.

10. **Blackburn H. M., Sherwin S. J.,** Instability modes and transition of pulsatile stenotic flow: pulse-period dependence, J. Fluid Mech. 573 (2007) 57–88.

11. **Varghese S. S., Frankel S. H., Fischer P. F.,** Direct numerical simulation of stenotic flows. Part 1. Steady flow, J. Fluid Mech. 582 (2007) 253–280.

12. **Varghese S. S., Frankel S. H., Fischer P. F.,** Direct numerical simulation of stenotic flows. Part 2. Pulsatile flow, J. Fluid Mech. 582 (2007) 281–318.

13. **Molla M. M., Paul M. C., Roditi G.,** LES of additive and non-additive pulsatile flows in a model arterial stenosis, Computer Methods in Biomechanics and Biomedical Engineering. 13 (1) (2010) 105–120.

14. **Paul M. C., Molla M. M.,** Investigation of physiological pulsatile flow in a model arterial stenosis using large-eddy and direct numerical simulations, Appl. Math. Model. 36 (9) (2012) 4393–4413.

15. **Gataulin Ya. A., Smirnov E. M.,** A flow in the blood vessel with a one-side stenosis: numerical study of the structure and local turbulization, St. Petersburg Polytechnical State University Journal. Physics and Mathematics. 14 (1) (2021) 72–84.

16. **Sukhapure K., Burnsa A., Mahmuda T., Spoonerb J.,** CFD modelling and validation of head losses in pipe bifurcations, In book: 13th International Conference on Heat Transfer, Fluid Mechanics and Thermodynamics. 489–494.

17. **Mikheev N. I., Dushin N. S.,** A method for measuring the dynamics of velocity vector fields in a turbulent flow using smoke image-visualization videos, Instruments and Experimental Techniques. 59 (6) (2016) 882–889.

18. **Germano M., Piomelli U., Moin P., Cabot W. H.,** A dynamic subgridscale eddy viscosity model, Phys. Fluids. 3 (7) (1991) 1760–1765.

19. **Lilly D. K.,** A proposed modification of the Germano subgrid-scale closure method, Phys. Fluids. 4 (3) (1992) 633–635.

20. **Jeong J., Hussain F.,** On the identification of a vortex, J. Fluid Mech. 285 (1995) 69–94.

СПИСОК ЛИТЕРАТУРЫ

1. **Schirmer C. M., Malek A. M.** Computational fluid dynamic characterization of carotid bifurcation stenosis in patient-based geometries // Brain and Behavior. 2012. Vol. 2. No. 1. Pp. 42–52.

2. **Filardi V.** Carotid artery stenosis near a bifurcation investigated by fluid dynamic analyses // Neuroradiology Journal. 2013. Vol. 26. No. 4. Pp. 439–453.

3. **Li C-H., Gao B-L., Wang Ji-W., Liu J-F., Li H., Yang S.-T.** Hemodynamic factors affecting carotid sinus atherosclerotic stenosis // World Neurosurgery. 2019. Vol. 121. Pp. 262–276.

4. **Haruguchi H., Teraoka S. J.** Intimal hyperplasia and hemodynamic factors in arterial bypass and arteriovenous grafts: a review // Artificial Organs. 2003. Vol. 6. No. 4. Pp. 227–235.

5. **McGah P. M., Leotta D. F., Beach K. W., Riley J. J., Aliseda A.** A longitudinal study of remodeling in a revised peripheral artery bypass graft using 3D ultrasound imaging and computational hemodynamics // Journal of Biomechanical Engineering. 2011. Vol. 133. No. 4. Pp. 1–10.

6. **Donadoni F., Pichardo-Almarza C., Bartlett M., Dardik A., Homer-Vanniasinkam S., Диаz-Zuccarini V.** Patient-specific, multi-scale modeling of neointimal hyperplasia in vein grafts // Frontiers in Physiology. 2017. Vol. 8. Pp. 1–10.

7. **Mittal R., Simmons S. P., Udaykumar H. S.** Application of large-eddy simulation to the study of pulsatile flow in a modelled arteria stenosis // Journal of Biomechanical Engineering. 2001. Vol. 123. No. 4. Pp. 325–332.

8. **Mittal R., Simmons S. P., Najjar F.** Numerical study of pulsatile flow in a constricted channel // Journal of Fluid Mechanics. 2003. Vol. 485. Pp. 337–378.

9. **Sherwin S. J., Blackburn H. M.** Three-dimensional instabilities and transition of steady and pulsatile flows in an axisymmetric stenotic flows // Journal of Fluid Mechanics. 2005. Vol. 533. Pp. 297–327.

10. **Blackburn H. M., Sherwin S. J.** Instability modes and transition of pulsatile stenotic flow: pulse-period dependence // Journal of Fluid Mechanics. 2007. Vol. 573. Pp. 57–88.

11. **Varghese S. S., Frankel S. H., Fischer P. F.** Direct numerical simulation of stenotic flows. Part 1. Steady flow // Journal of Fluid Mechanics. 2007. Vol. 582. Pp. 253–280.

12. **Varghese S. S., Frankel S. H., Fischer P. F.** Direct numerical simulation of stenotic flows. Part 2. Pulsatile flow // Journal of Fluid Mechanics. 2007. Vol. 582. Pp. 281–318.

13. **Molla M. M., Paul M. C., Roditi G.** LES of additive and non-additive pulsatile flows in a model arterial stenosis // Computer Methods in Biomechanics and Biomedical Engineering. 2010. Vol. 13. No. 1. Pp. 105–120.

14. **Paul M. C., Molla M. M.** Investigation of physiological pulsatile flow in a model arterial stenosis using large-eddy and direct numerical simulations // Applied Mathematical Modelling. 2012. Vol. 36. No. 9. Pp. 4393–4413.

15. **Гатаулин Я. А., Смирнов Е. М.** Численное исследование структуры и локальной турбулизации течения в кровеносном сосуде с односторонним стенозом // Научно-технические ведомости СПбГПУ. Физико-математические науки. 2021. Т. 14. № 1. С. 72–84.

16. **Sukhapure K., Burnsa A., Mahmuda T., Spoonerb J.** CFD modelling and validation of head losses in pipe bifurcations // 13th International Conference on Heat Transfer, Fluid Mechanics and Thermodynamics. Pp. 489–494.

17. **Михеев Н. И., Душин Н. С.** Метод измерения динамики векторных полей скорости турбулентного потока по видеосъемке дымовой визуализации // Приборы и техника эксперимента. 2016. № 6. С. 114–122.

18. **Germano M., Piomelli U., Moin P., Cabot W. H.** A dynamic subgridscale eddy viscosity model // Physics of Fluids. 1991. Vol. 3. No. 7. Pp. 1760–1765.

19. **Lilly D. K.** A proposed modification of the Germano subgrid-scale closure method // Physics of Fluids. 1992. Vol. 4. No. 3. Pp. 633–635.

20. **Jeong J., Hussain F.** On the identification of a vortex // Journal of Fluid Mechanics. 1995. Vol. 285. Pp. 69–94.

THE AUTHORS

GATAULIN Yakov A.
Peter the Great St. Petersburg Polytechnic University
29 Politechnicheskaya St., St. Petersburg, 195251, Russia
yakov_gataulin@mail.ru
ORCID: 0000-0002-0200-6508

SMIRNOV Evgueni M.
Peter the Great St. Petersburg Polytechnic University
29 Politechnicheskaya St., St. Petersburg, 195251, Russia
emsmirnov2003@mail.ru
ORCID: 0000-0002-7218-6372

MOLOCHNIKOV Valery M.
Kazan National Research Technical University named after A. N. Tupolev – KAI
10, K. Marx St., Kazan, Tatarstan, 420111, Russia
vmolochnikov@mail.ru
ORCID: 0000-0001-8182-6856

MIKHEEV Andrei N.
Federal Research Center 'Kazan Scientific Center of the Russian Academy of Sciences'
2/31, Lobachevsky St., Kazan, Tatarstan, 420111, Russia
AndreiRonnieMiheev@yandex.ru
ORCID: 0000-0002-8687-8994

СВЕДЕНИЯ ОБ АВТОРАХ

ГАТАУЛИН Яков Александрович – *ассистент Высшей школы прикладной математики и вычислительной физики Санкт-Петербургского политехнического университета Петра Великого.*
195251, Россия, г. Санкт-Петербург, Политехническая ул., 29
yakov_gataulin@mail.ru
ORCID: 0000-0002-0200-6508

СМИРНОВ Евгений Михайлович – *доктор физико-математических наук, профессор Высшей школы прикладной математики и вычислительной физики Санкт-Петербургского политехнического университета Петра Великого.*
195251, Россия, г. Санкт-Петербург, Политехническая ул., 29
emsmirnov2003@mail.ru
ORCID: 0000-0002-7218-6372

МОЛОЧНИКОВ Валерий Михайлович – *доктор технических наук, профессор Казанского национального исследовательского технического университета имени А. Н. Туполева – КАИ.*
420111, Россия, Республика Татарстан, г. Казань, ул. К. Маркса, 10
vmolochnikov@mail.ru
ORCID: 0000-0001-8182-6856

МИХЕЕВ Андрей Николаевич – *кандидат технических наук, научный сотрудник Федерального исследовательского центра «Казанский научный центр Российской академии наук».*
420111, Россия, Республика Татарстан, Казань, ул. Лобачевского 2/31
AndreiRonnieMiheev@yandex.ru
ORCID: 0000-0002-8687-8994

Received 01.10.2022. Approved after reviewing 17.10.2022. Accepted 17.10.2022.
Статья поступила в редакцию 01.10.2022. Одобрена после рецензирования 17.10.2022. Принята 17.10.2022.